Molecular dynamics simulations of atomic-level brittle fracture mechanisms in amorphous silica

**Krishna Muralidharan · Ki-Dong Oh ·
P. A. Deymier · K. Runge · J. H. Simmons**

Abstract We have examined the atomic dynamics of the brittle fracture process in amorphous silica using molecular dynamics. Under strain, extensive atomic restructuring occur in the vicinity of voids leading to the formation of 2-membered (2-M) silica rings that are much different than the open network structure of the bulk. The sequence of events that lead to the formation of the 2-M rings was characterized by examining the change in local coordination of atoms.

Introduction

The brittle fracture process has been a subject of many modeling and experimental efforts, but the fundamental atomic level processes governing brittle fracture have not been well understood. Unlike in ductile materials, where there is considerable plastic deformation prior to failure and consequently an amount of predictability, brittle fracture is sudden and rapid. When brittle materials are subjected to dynamic loads, failure occurs due to the rapid propagation of cracks, and in the absence of a dominant crack, we see spalling of the material due to the nucleation, growth and coalescence of multiple flaws (cracks, voids,

etc.). In both cases, we can expect the dominant failure processes to be the same [1].

Early modeling efforts based on the work of Griffith predicted the mechanical properties of materials with sharp cracks [2–7]. Though useful in their ability to calculate the energetics of the macroscopic fracture event, these methods were inadequate to describe atomic-level processes. Later, with the advent of fast and powerful computers, atomistic computational techniques like molecular dynamics (MD) were used to study brittle fracture of both crystalline (like Si) and amorphous materials (like amorphous silica). Some MD simulations [8–16] mimicked typical experimental studies [17–24] by studying materials with a primary crack in their simulated samples, while other MD studies [25–29] used crack-free samples of sizes < (5,000 atoms) in their simulations. Typically, the smaller-size-MD simulations were subjected to uniform strain rates, with the strain being applied uniformly throughout the material, while the bigger samples containing cracks were subjected to external strain via displacement of boundary atoms if periodic boundary conditions (PBC) were not imposed. Despite the very different nature of the two kinds of simulations (discussed in a later section), a common theme among them, especially in fracture studies of amorphous materials like silica glass was the formation and coalescence of nanoscale and sub-nanoscale voids (as opposed to much larger voids in plastic deformation of ductile metals) leading to fracture [8, 16, 25–29] as also seen in experiments [30, 31]. Still, a clear picture of the exact nature of the atomic mechanisms governing the formation of the voids and consequently brittle fracture has not yet emerged. Thus, a primary objective of this work is to accurately document and characterize in detail the atomic dynamics occurring in brittle materials as they fracture. In order to carry out the investigations, we use MD simulations as a probe to study

K. Muralidharan (✉) · K.-D. Oh · P. A. Deymier ·
J. H. Simmons
Department of Materials Science and Engineering, University of Arizona, Mines Building, Tucson, AZ 85721, USA
e-mail: krishna@qtp.ufl.edu

K. Muralidharan · K. Runge
Quantum Theory Project, University of Florida, New Physics Building, Gainesville, FL 32611, USA

the fracture characteristics of amorphous silica (a-SiO$_2$), a 'model' brittle material. Extensive experimental as well as simulation literature is available on a-SiO$_2$, as it is an important technological material [32]. In our studies, we study environment-independent fracture, and therefore the effect of moisture is ignored.

Background

In this section, an overview of past MD and experimental studies that examined atomic-level fracture processes in brittle materials will be given.

MD simulations of brittle fracture

MD is a simulation technique for computing the thermodynamic as well as kinetic properties of a classical many-body system [33]. The most critical component of an MD simulation is the interatomic potential. Recent advances in quantum computational methods have led to the development of accurate semi-empirical potentials that are parameterized to represent 'important' equilibrium properties of the material. But, fracture is a non-equilibrium process, and even MD simulations that use accurately parameterized interatomic potentials may yield results that do not match experimental observations. In fact, Hauch et al. have compared the energetics of crack propagation in silicon using both experiments and MD simulations, and have found quantitative differences in the results of simulations and experiments [21]. Despite the reservations regarding the accuracy of MD simulations, a careful interpretation of results keeping in mind the limitations of the potentials will go a long way in understanding the brittle fracture process.

Research groups that have used MD to examine brittle fracture [8–16, 25–29] primarily focused on examining environment independent fast-fracture in brittle materials as the timescale governing environment dependent fracture processes (crack speeds < 10^{-6} m/s) are beyond MD timescales. Theoretical calculations involving quantum mechanical (QM) computations have studied the effect of moisture (and other environments) on the fracture process in brittle materials like a-SiO$_2$. These calculations were carried out at 0° K, and atomics dynamics were not explicitly included [34–37].

Soules and Busby [25] examined sodium silicate glasses consisting of 1,000–2,000 atoms with free surfaces under both tension and compression. They noticed that under biaxial expansion, the sample was drawn thinner, and when the expansion was large, the sample failed via void formation and cavitation. Keiffer and Angell [38] noticed a self-similar void structure in silica glass when the material was subjected to sudden isotropic expansion. Ochoa et al. [26–28] and Swiler et al. [29] examined a-SiO$_2$'s structure as a function of uniaxial strain-rate and noticed the formation and coalescence of sub-nanoscale voids with increasing strain. This was accompanied by a non-trivial amount of plastic deformation in the form of bond-breakage and atomic rearrangement. In their studies, strain was applied uniformly throughout the sample, which consisted of 1,000–2,000 atoms with periodic boundaries. They concluded that strain was relieved via alignment of individual silica tetrahedra with the direction of applied strain through thermal vibrations. It has to be pointed out that the strain rates used in the above simulations (>0.01/ps) are generally beyond experimental strain rates. Van Brutzel et al. [16] performed multi-million atom simulations on a-SiO$_2$ to study the propagation of a crack in the medium by uniaxially straining the boundary atoms of the material and observed formation of nanoscale voids and pores (40–50 nm in radius) in low density regions in front of the propagating crack-tip. Recent investigations have indicated that the growth of 'critical' voids could be correlated to the stress response of a-SiO$_2$ as it is uniaxially strained [39]. Specifically, when the material responds elastically to the applied strain, elastic deformation of voids is seen. Once the material begins to separate, critical voids grow rapidly, sometimes via the coalescence of surrounding 'satellite' voids.

All the above discussed MD simulations clearly indicate the formation of voids with increasing strain, with the size of the largest voids scaling with the respective sample size. Another key observation of the above MD simulations was that the material failed at different strains, depending on the nature of the sample. In the case of Van Brutzen et al., the presence of a crack resulted in the material failing at much lower strains (~6%) when compared to the simulations of Ochoa et al. and Swiler et al., where the much smaller crack-free sample (with PBC) failed at much larger strains (~30%). Ochoa et al. noticed spalling of the crack-free samples, while in the case of Van Brutzen et al., the dominant process was controlled by crack propagation. It should be noted that the work of Van Brutzen et al. is closer to typical experimental studies of brittle fracture, where the failure process is dominated by the presence of flaws, while the method of Ochoa et al. represents strain-rates not normally achievable in experiments, except in cases like shocking of materials.

Past experimental investigations

Until recently, experiments almost always used optical techniques to study atomic level processes in material fracture [discussed in Ref. 1]. However, these lacked the spatial and temporal resolution to accurately characterize

atomic dynamics. The advent of high-resolution atomic force microscopy (AFM) and scanning tunneling microscopy (STM) has resulted in some important observations of the brittle fracture process. Guilloteau et al. [30] used AFM to examine the core region surrounding a propagating crack-tip in the sub-critical regime (crack velocity < 10^{-6} m/s) in soda-lime glass and noticed that there was considerable plastic deformation around the vicinity of the flaw even in brittle materials. Celarie et al. [31] in similar fashion examined brittle fracture in aluminosilicate and silica glass surfaces and concluded that slow fracture was not composition dependent and progressed via the nucleation, growth and coalescence of nanoscale voids (and cavities). They further stated that the formation of these cavities was due to the amorphous nature of the materials and the inherent fluctuations in the local atomic density at the nanometer scale.

Simulation procedure

The above discussions on MD fracture simulations point out that using dissimilar methodologies to study fracture leads to clear differences in some of the results obtained such as (i) spalling versus crack propagation, and (ii) value of failure strain, though the nature of failure (via void formation and coalescence) is still the same. Since the main objective of this work is only to document the atomic mechanisms that govern brittle fracture in a-SiO$_2$ and not make quantitative predictions about the energetics of the failure process, we follow the computationally less-intensive methodology of Ochoa et al., to study the dynamics of silica glass samples with the implicit assumption that the fundamental atomic mechanisms remain the same. In other words, we use small MD samples with PBC that are flaw-free at a scale comparable to the dimensions of the MD cell. The samples are subjected to constant strain rates with the strain applied uniformly throughout the sample.

Typically in MD simulations, silica glass is prepared by quenching liquid SiO$_2$. In our case, a β-cristobalite sample consisting of 3528 atoms was heated above 8,000 K and quenched to 300 K at a cooling rate of 125 K/ps as prescribed by Huff et al. [40]. The interatomic interactions were represented by a modified BKS potential derived from ab initio calculations [41]. The original BKS potential formulated by van Beest et al. was derived from restricted Hartree-Fock (RHF) cluster calculations. They considered a H$_4$SiO$_4$ molecule and generated the energy surface by symmetrically stretching the Si–O bonds and making the oxygen atoms bend towards each other. We use a modified form of the BKS potential as proposed by Corrales [41] to avoid unphysical effects at small interatomic distances that arise in the original BKS potential. The form of the modified potential is given below (Eq. 1), with the parameters listed in Table 1.

$$\phi_{ij} = \frac{q_i q_j}{r_{ij}} + A_{ij}\exp(-b_{ij}r_{ij}) - \frac{c_{ij}}{r_{ij}^6} + 4\varepsilon_{ij}(\frac{\sigma}{r_{ij}})^{12} - 4\varepsilon_{ij}(\frac{\sigma}{r_{ij}})^6,$$

where ϕ_{ij} is the potential energy corresponding to an interatomic separation of r_{ij} between atoms i and j. Ewald summation [42] was used to ensure a rapid convergence of the coulombic contribution to the total potential energy of the system. The fictive glass transition temperature was found to be 3125 ± 20 K. The sample was equilibrated at 300 K under NPT conditions (using a Nose-Hoover thermostat and barostat [43, 44]) to ensure zero pressure. The dimensions of the resultant sample were 37 Å in each direction, with the density (2.28 g/cc) close to experimental value. The radial distribution functions (RDF) and the bond angle distributions (BAD) of the glass were consistent with experimental data [45]. Glasses consisting of 2,940 and 3,024 atoms were also prepared and the resultant density, RDF, and BAD of each glass were very similar. In our studies, we will be presenting results of simulations conducted on the primary sample (3,528 atoms). Uniaxial strain rates ranging from 0.1/ps to 0.0001/ps were imposed on the sample in each of the x, y and z directions and the stress response (calculated via the virial theorem [46]) was found to be perfectly isotropic. We did not simulate strain rates below 0.0001/ps as results indicated that there were no significant differences in the fracture strength between this trial and higher strain-rate simulations (<0.02/ps). Further, the atomic mechanisms that controlled the fracture process were identical for all strain rates as discussed below.

Results and discussions

Figure 1 shows the 300 K uniaxial stress-strain curves at various strain-rates. As pointed out in the figure, each stress-strain curve has 4 distinct regions (discussed in Ref. [39]), with an initial elastic region, followed by plastic 'flow' of the material (region II and III), and finally formation of fractured free surfaces (region IV). At lower strain rates (<0.01/ps) the maximum fracture strength is independent of the strain rate (~17 GPa), while at higher strain rates, the fracture strength increases with increasing strain-rate as also seen by Ochoa et al. Experimental fracture strength at very low temperatures and humidity of high-purity silica glass fibers have been determined to equal 12–15 GPa, and the limiting tensile strain has been reported to be anywhere from 0.18 to 0.21 [47–49], while there has a been a bit of uncertainty regarding the estimation of the experimental failure strain as discussed in

Table 1 Parameters used in the modified BKS potential

Interaction type	Parameters				
	A_{ij} (eV)	b_{ij} (Å^{-1})	c_{ij} (eV/Å^6)	ε_{ij} (eV)	σ_{ij} (Å)
Si–O	18003.7572	4.8732	133.5381	1.12245×10^{-2}	1.3100
O–O	1388.7730	2.7600	175.0000	3.5653×10^{-4}	2.2000
Si–Si	–	–	–	12.6387	0.4200

Fig. 1 Uniaxial Stress–Strain Curves for the BKS glass at 300 K. The 'region' labels are specific for the 0.10/ps case
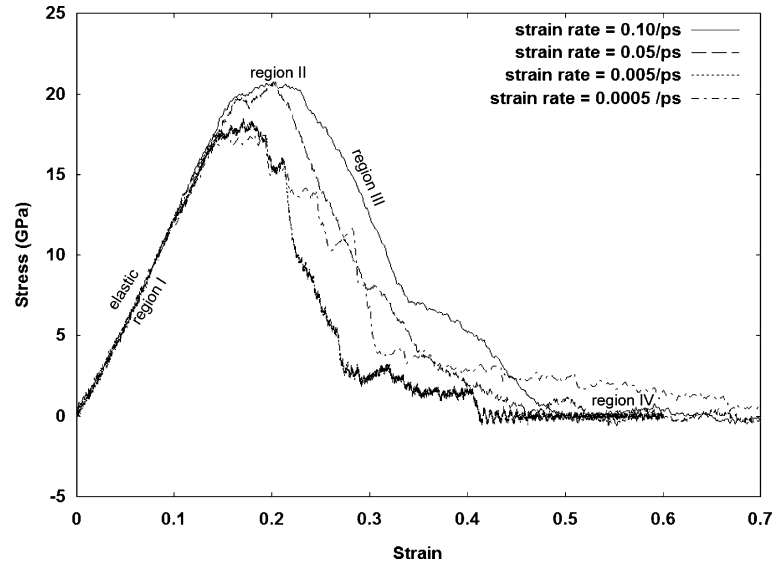
Ref. [50]. Typical fracture strain in our simulations occurs at strains around 0.30 (onset of region IV). Assuming that experimental fracture strains of silica fibers can be approximated by their tensile strain, the overestimation of the fracture strain in our simulations can be attributed to the fact that our samples are strictly flaw-free and also due to the method of applying uniform strain throughout the material thereby over-constraining the material leading to a higher fracture strain. Nevertheless, the fact that the stress response to external strain is similar for the various strain rates that differ by four orders of magnitude (0.1–0.0001/ps) lends credence to our assumption about the fundamental fracture mechanisms being invariant.

In order to characterize the atomic rearrangement mechanisms that occur as we strain the sample, we looked for some distinct 'signatures' that could be related to the stress-strain curves. This included examining the change in coordination of atoms and the evolution of RDF's and BAD's as a function of strain for the various strain rates. In region I, the entire material experiences the external strain via the elastic extension of Si–O bonds. It is only beyond the elastic region that we see substantial restructuring as discussed below.

Figure 2a and b represents the Si–O–Si and O–Si–O BAD as a function of strain for a sample strain rate = 0.01/ps. It is clear in both figures that features (peaks) start

developing between 80° and 100°, at strains corresponding to region III, implying possible structural rearrangement. Specifically, this could be related to local corner-sharing to edge-sharing transformations that occur in certain regions as the material is strained beyond a specific value of strain (onset of region III). In other words, in these critical regions, the local structure is characterized by edge-sharing tetrahedra, where neighboring silica tetrahedra share two oxygens rather than a single corner-sharing oxygen characteristic of bulk silica. The above observation is also reflected in the formation of new peaks at around 2.5 Å in the Si–Si RDF at high strains (Fig. 3), characteristic of edge-sharing silica tetrahedra (referred to as two membered (2-M) rings in literature). In addition, at these high strains, the rest of the material recovers to the equilibrium structure as reflected in the fact that the Si–O first neighbor RDF peak moves back to the equilibrium separation distance (~1.6 Å), and that Si–O–Si BAD peak goes back to its equilibrium angle (144°). Restating the above observations, one could conclude that in critical regions there is a structural transformation as the material becomes highly strained, while the rest of the material recovers (bulk recovery).

The formation of 2-M rings in silica has been under scrutiny in recent times [51–55] and it has been shown that the 2-M ring (consisting of 2 Si and 2 O atoms) is a highly

Fig. 2 Evolution of (**a**) O–Si–O BAD and (**b**) Si–O–Si (BAD) as a function of strain at a strain-rate = 0.01/ps
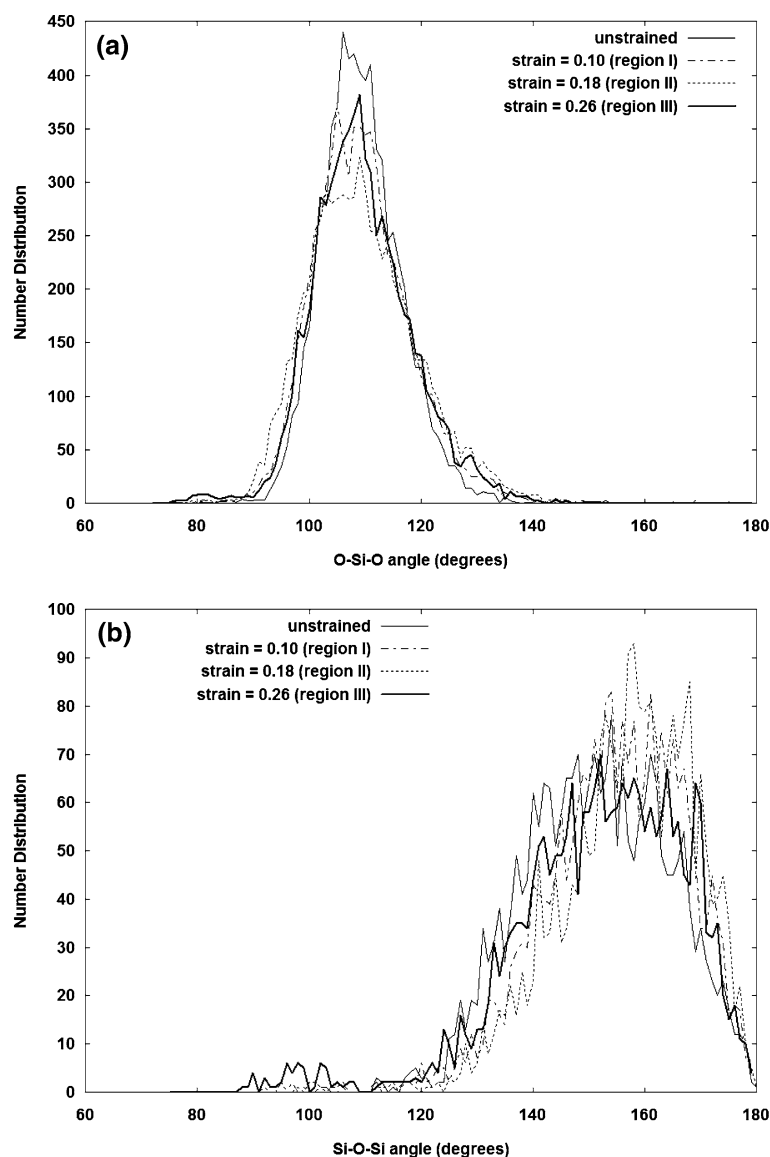
strained structure that is unstable in the presence of water molecules. In addition, Roder et al. had observed the formation of 2-M rings on dry amorphous silica surfaces in their MD simulations that also used the BKS potential [53]. Similarly, we too found that the fractured surfaces (region IV) were rich in 2-M rings. This result is not too surprising though, as one would expect a more planar network structure consisting of compact edge-sharing tetrahedra on a 2-D surface rather than the bulk 3-D corner-sharing structure. In other words, a 2-D surface is able to accommodate the highly strained 2-M ring structure probably because it is energetically viable. We use the word 'probable' as we will not attempt to calculate the energetics of the above process, and defer it to a later study.

The logical next step was to carefully study the evolution of the number of 2-M rings as a function of strain for the various strain-rates. Figure 4 shows the number evolution of 2-M rings for two sample strain rates, 0.01/ps and 0.05/ps. It is evident that there are very few 2-M rings in region I and II and past region II, there is a dramatic increase in the number of 2-M rings. Also, once the material separates (region IV), there is a clear saturation in the abundance of the 2-M rings. Structural characterization of the glass structure showed that most of the 2-M rings were located in the vicinity of prominent voids in region III, and close to the fractured surface in region IV.

In the above discussion, we had referred to 'prominent voids' and the abundance of 2-M rings in their vicinities. In the following brief discussion we will make our meaning more precise. In general, the open network structure of a-SiO$_2$ leads to a distribution of voids throughout the material (In our simulations, we approximate the voids by

Fig. 3 Evolution of Si–Si first neighbor RDF as a function of strain at a strain-rate = 0.01/ps
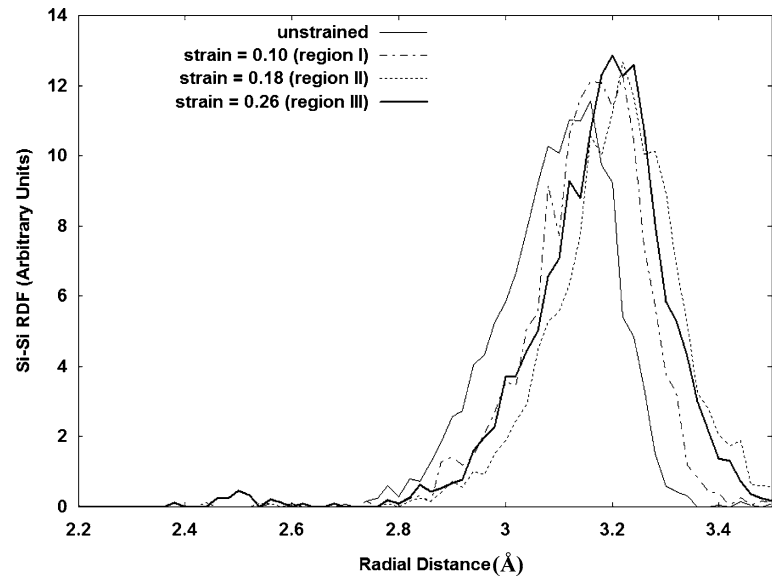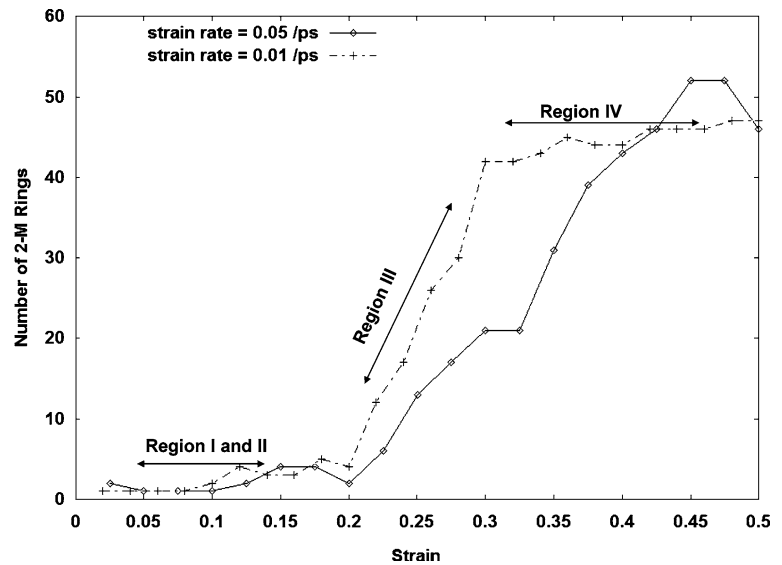

Fig. 4 Number distribution of the 2-M rings as a function of strain at two different strain rates (0.01/ps and 0.05/ps)

spheres; the methodology of doing the void analysis is discussed in Ref. [39]). As we strain the material, all voids initially strain elastically. Past region II, some voids (i.e., prominent voids) grow more rapidly than others and most of these big voids then form a network leading to the separation of the material and formation of the fracture surfaces (Fig. 5).

Figure 6a depicts the size of the biggest void (BV) as a function of strain for all strain rates. One has to note that the above plot does not explicitly track one specific void, but only refers to the biggest void at that particular value of strain. Thus, a scenario could arise where a momentary BV may not be part of the network of voids that leads to the separation of the material. In general, past region II, all prominent network voids grow rapidly in a fashion

similar to Fig. 6a. Figure 6b and c shows the evolution of the void-size distribution as a function of strain for strain-rate = 0.0001/ps; at strains corresponding to regions I and II (Fig. 6b), the number of small voids (<2.4 Å) decreases with increasing strain, while there is a steady and gradual increase in the number of bigger voids, with a consequent increase in the size of the biggest void. Past region II (Fig. 6c), there is a significant increase in the rate of growth of the bigger voids, with the number of smaller voids also increasing at higher strains (strain = 0.27 in Fig. 6c).

Figure 6a and c point out the fact that there is a rapid increase in the rate of growth of BV (as also other big/prominent voids) at around the onset of region III. Keeping this in mind and the fact that there is a corresponding rapid
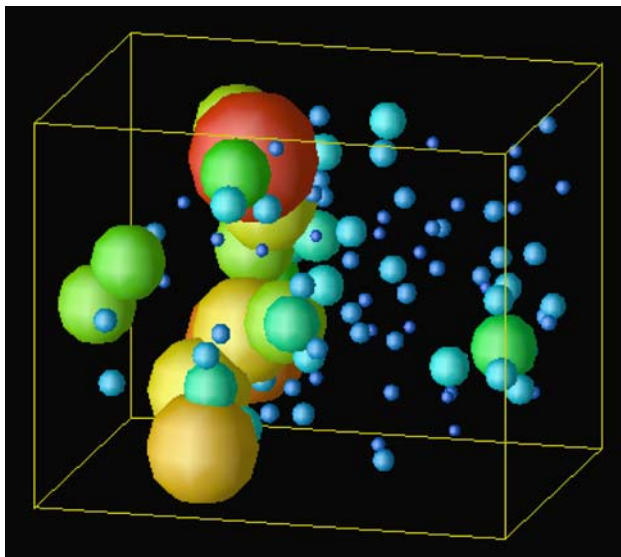
Fig. 5 Network of voids that interconnect leading to separation of the material. The voids form a network perpendicular to the straining direction. The voids are color-coded such that the biggest void(s) is red while the smallest voids are blue

increase in the number of 2-M rings, one can draw a logical conclusion that past a critical size, the BV's surface becomes a virtual free surface, thereby hastening the formation of the 2-M structures. Thus atomic rearrangement around BV (and other prominent voids) occurs via local transformation from a corner-sharing to an edge-sharing structure. As this transformation proceeds in the critical regions (around the prominent voids), the voids simultaneously grow due to local change in structure. Thus the fracture process in the critical regions proceeds via a two-step feedback mechanism, which consists of (i) atomic rearrangement and restructuring on and around a void's surface area, and (ii) growth of the void via reordering of the 'local' structure. Simultaneously, past a critical strain, there is bulk recovery in rest of the material. Finally, the material separates when critical voids form an interconnected network or a single critical void grows, such that the length of the void(s) extends across the dimensions that are perpendicular to the uniaxial strain direction of the material. This leads to the formation of two sub-materials, whose surface structure is vastly different from the bulk structure.

Having discussed the fact that the 2-M rings are found in close proximity to big voids, we next study the exact nature of the transformation that leads to the formation of 2-M rings. The following set of figures- (Fig. 7a–c) illustrate the above and show the evolution of local structure in a-SiO_2 when subjected to a strain rate = 0.01/ps. Specifically, we
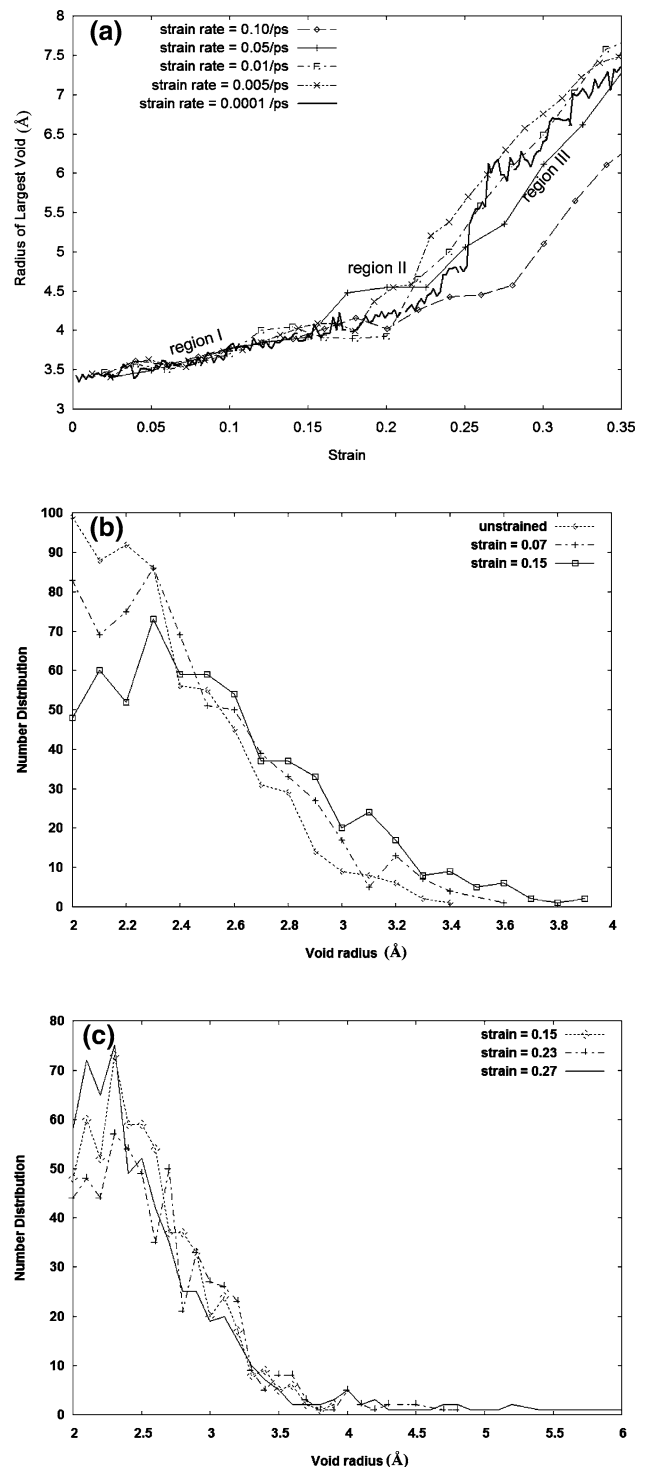

Fig. 6 (**a**) Growth of the BV as a function of strain for different strain-rates. The 'region' labels are specific for the 0.05/ps case. (**b**) Void size distribution as a function of strain for a strain rate = 0.0001/ps. The strains correspond to region I and II. (**c**) Void size distribution as a function of strain for a strain rate = 0.0001/ps. The strains correspond to region III though we have also presented strain = 0.15 (region I) for reference

Fig. 7 Snapshots of the 'local' structure—(**a**–**c**) of the 'BKS' glass when subjected to a strain rate = 0.01/ps. The snapshots were recorded at strains equaling 0.18, 0.19 and 0.23, respectively. The red atoms are oxygens and blue indicates silicon atoms
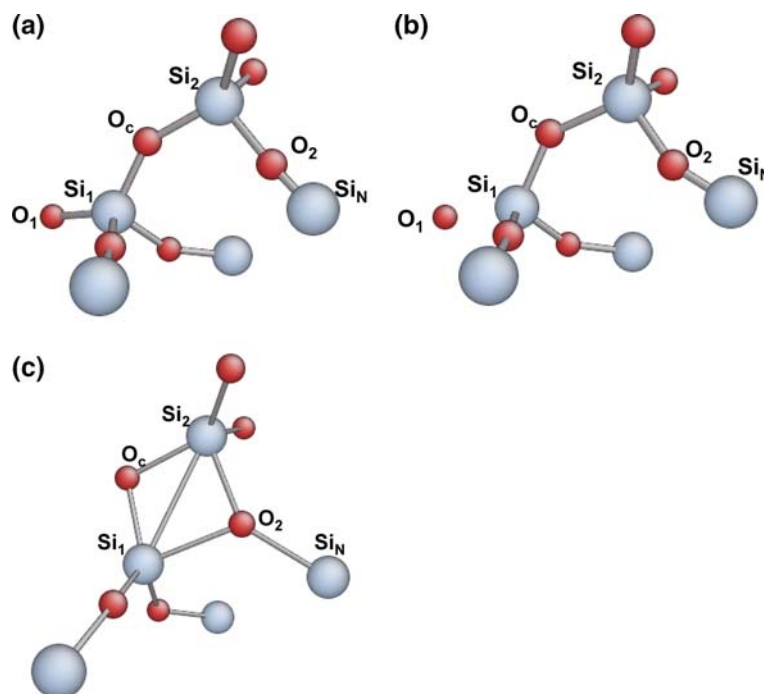
track two neighboring silica tetrahedra that initially share a common oxygen atom and later form a 2-M ring (i.e., share two common oxygen atoms).

Figure 7a shows two Si atoms- Si_1 and Si_2 (as indicated in the figure) that share a common ''corner'' oxygen atom (Oc). As the material is strained, one of the oxygen neighbors (O_1) of Si_1 ceases to be a neighbor as shown in Fig. 7b (we define a Si atom and an oxygen atom to be neighbors if their distance of separation is <2 Å), and Si_1 becomes 3-coordinated, while O_1 becomes 1-coordinated. At a slightly higher strain, Si_1 acquires a new neighbor (O_2), which results in the formation of the 2-M ring (Fig. 7c).

A more detailed examination of the process indicates that the transformation is rapid; within a strain increment of 0.01, the bond distance between Si_1 and O_1 goes from 1.78 Å to 2.23 Å, and then within the next successive 0.01 strain increment, the distance of separation becomes >3.5 Å. Due to the bond breaking, both atoms acquire a great amount of energy resulting in rapid motion of the two atoms. This results in Si_1 atom being 3-coordinated temporarily until it acquires O_2 as a neighbor to make it 4-coordinated. During the period that Si_1 is 3-coordinated, Si_1 and its three oxygen neighbors form an almost planar structure. Once Si_1 becomes 4-coordinated, there is an inversion in the corresponding tetrahedron's orientation. As the 2-M ring is formed, O_2 becomes 3-coordinated, with its neighbors being Si_1, Si_2 and Si_N, as shown in Fig. 7c. Before the formation of the 2-M ring, O_2 was coordinated only to Si_N and Si_2.

Though we discussed a very specific case to illustrate the formation of a 2-M ring, in general, the formation of all 2-M rings with increasing strain can be represented by the above discussed mechanism that involves forming 1-coordinated oxygen atoms (1-C O), 3-coordinated silicon atoms (3-C Si) and then 3-coordinated oxygen atoms (3-C O) as seen in the following figures.

Figures 8a and b present the number distribution of the 2-M rings and the number of non-regular coordination states of the atoms as a function of strain at 0.01/ps and 0.05/ps, respectively. By 'non-regular' we refer to the silicon and oxygen atoms that are not in their normal coordination states (4 and 2 are the normal coordination states of silicon and oxygen respectively). From the two figures it is clear that the number of 1-C oxygen atoms and 3-C silicon atoms increases rapidly between the onsets of region II and region III. This corresponds to the fact that some Si–O bonds are broken leading to the change in the coordination of the respective atoms. The fact that the number of 1-C oxygen atoms is greater than the number of 3-C silicon atoms is because some of the silicon atoms that lost an oxygen neighbor were already 5-coordinated. In addition, some of the 3-C silicon atoms rearranged rapidly to become 4-coordinated once again, with a small fraction of these atoms forming 2-M rings (corresponding to a small increase in the number of 2-M rings in region II).

Past the onset of region III, the number of 2-M rings and the number of 3-C oxygen atoms increase rapidly. As shown previously in Figs. 7a–c, this corresponds to the fact

Fig. 8 Variation of the number of 2-M rings and the number of non-regular coordinated atoms as a function of strain at (**a**) strain rate = 0.01/ps, and (**b**) strain rate = 0.05/ps
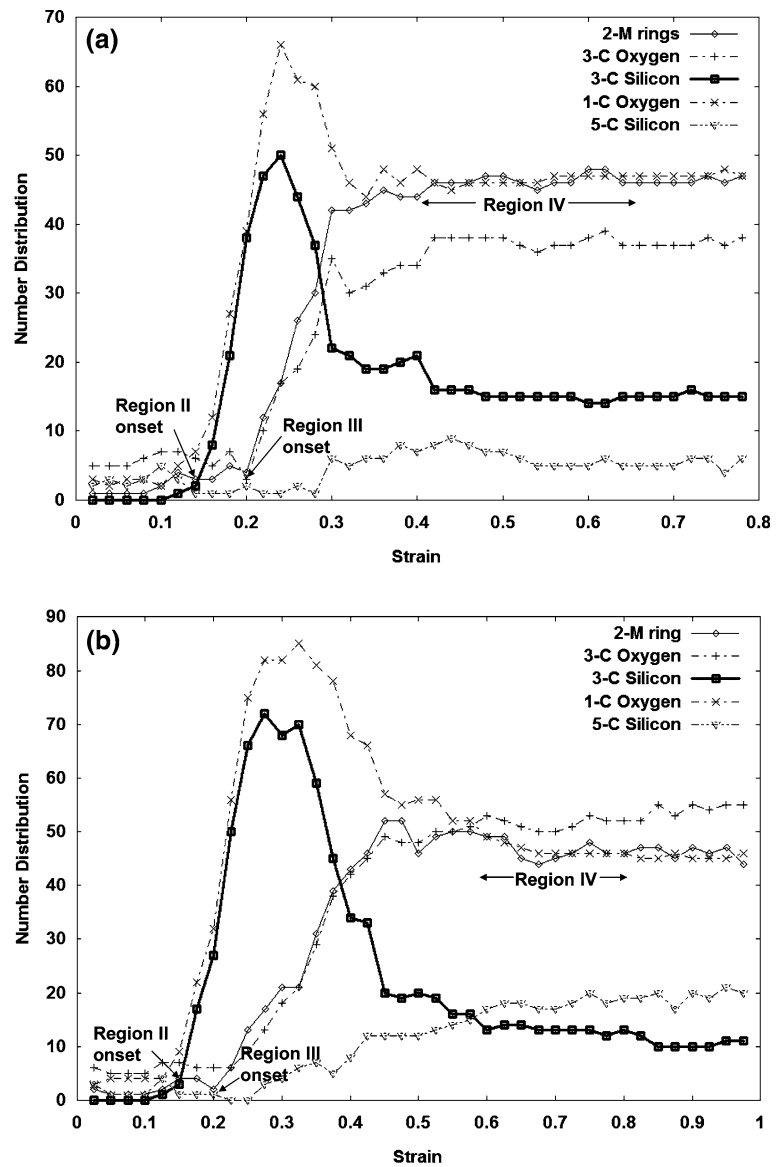
that the 3-C silicon atoms become 4-coordinated once again by forming 2-M rings. This results in one of the oxygen atoms (belonging to the 2-M ring) becoming 3-coordinated. Also, not all 3-C silicon atoms get converted to 2-M rings. In region IV, the number of 2-M rings and the number of 3-C oxygen atoms saturate.

Just beyond the onset of region III, the number of 1-C oxygen atoms and the number of 3-C silicon atoms reach a maximum. Then, there is a subsequent decrease with the number distribution saturating in region IV. Interestingly, the number of 1-C oxygen atoms is almost identical to the number of 2-M rings in region IV. This implies that only some 1-C oxygen atoms rearrange to become 2-coordinated, while the majority (initially coordinated to silicon atoms that subsequently form 2-M rings) remain in the same state. Almost all of these 1-C oxygen atoms are found

close to the fracture surfaces. The 1-C oxygen atoms that rearrange coordinate with either 4-coordinated silicon atoms (resulting in an increase in 5-C Si) or with some of the 'unconverted' 3-C silicon atoms (resulting in a decrease in the 3-C Si).

A comparison between the number of 3-C silicon atoms at 0.01/ps and 0.05/ps as a function of strain shows that the maximum number of 3-C silicon atoms at 0.05/ps is much larger. This is due to the fact that at smaller strain-rates, more 3-C silicon atoms (with respect to 0.05/ps) are able to rearrange to become 4-coordinated once again. In contrast, in the later stages of fracture (region IV), the number of remaining 'unconverted' 3-M silicon atoms is slightly larger at 0.01/ps. This can be attributed to the fact that at lower strain-rates, some 3-C oxygen atoms (belonging to 2-M rings) relax structurally to 'break away' from the

neighboring silicon that is not associated with the 2-M ring. This leads to the creation of 3-C silicon atoms and a decrease in the number of 3-C oxygen atoms (the 3-C O becomes 2-coordinated). Thus, the number of 3-C oxygen atoms at the lower strain-rate is smaller than the number of 2-M rings. At 0.05/ps, the number of 3-C oxygen atoms is identical to the number of 2-M rings up to region IV. In region IV, initially the number distributions are similar, while later, the number of 3-C oxygen atoms slightly increases. The additional number of 3-C oxygen atoms corresponds to the relatively large (compared to 0.01/ps) increase in the number of 5-C silicon atoms signifying that some of the 2-C oxygen atoms in the bulk acquire an additional silicon neighbor leading to an increase in 3-C oxygen and 5-C silicon atoms. In fact, the number of 5-C silicon atoms becomes larger than the number of 3-C silicon atoms.

Also, the maximum number of 2-M rings in both cases is almost identical, meaning that the 'efficiency' of conversion of 3-C silicon atoms to 2-M rings is much higher at lower strain-rates. The fact that the number of 2-M rings in both cases is comparable in region IV indicates that the nature of the fracture surfaces formed is similar at the two strain-rates, given that the 2-M rings are found predominantly close to the fracture surface.

The above discussed atomic restructuring mechanisms that take place past the elastic region, account for the plastic flow that we observe in the stress-strain curves. The plastic deformation consists of a simultaneous growth of 2-M rings and voids. The identification of this mechanism is of critical importance for understanding the precise nature of atomic-level mechanisms that govern brittle fracture in a-SiO$_2$.

Conclusions

Past simulational and experimental work on brittle fracture have indicated the formation of nanoscale and sub-nanoscale voids as the material fractures. The objective of this work was to exactly characterize the nature of the atomic-level mechanisms that result in void formation. Using MD, we have pointed out the sequence of atomic-scale events that occur when a brittle material that is uniaxially strained, fractures. Specifically, we have seen that at high strains (region III and beyond), there are localized transformations from a corner-sharing to edge-sharing structures (2-M rings) in the vicinity of large voids. Surfaces of critical voids become nucleation centers for the formation of 2-M rings. Once the 2-M rings form, there is compaction of the local structure around the voids resulting in a further growth of the voids. The formation of the 2-M rings is due to extensive local restructuring involving the creation of

1-C O atoms and 3-C Si atoms. The 3-C Si atoms then predominantly rearrange to form 2-M rings.

The accuracy of the observations and inferences made in this paper depend on the ability of the BKS potential to describe configurations far from equilibrium that arise in a typical fracture process. Nevertheless, the above findings represent an important first-step in completely documenting the brittle fracture mechanisms. Future work would involve experimental validation of these observations and studying the fracture process in a-SiO$_2$ using a wide variety of potentials as well as characterizing fracture in other brittle materials.

References

1. Ravi-Chandar K (1998) Int J Fracture 90:83
2. Griffith AA (1920) Phil Trans Roy Soc A221:163
3. Inglis CE (1913) Trans Int Naval Arch London V.LV:219
4. Lawn B In: Fracture of brittle solids, Cambridge Solid State Science Series, 2nd edn., p 33
5. Irwin GR (1957) J Appl Mech 24:361
6. Orowan E (1942) Repts Prog Phys 12:185
7. Barenblatt GI (1962) Adv Appl Mech 7:55
8. Rountree CL, Kalia RK, Lidorikis E, Nakano A, Van Brutzel L, Vashishta P (2002) Annu Rev Mater Res 32:377
9. Holland D, Marder M (1998) Phys Rev Lett 80:746
10. Swadener JG, Baskes MI, Nastasi M (2002) Phys Rev Lett 89:855031
11. Holian BL, Ravelo R (1995) Phys Rev B 51:11275
12. Abraham FF, Brodbeck D, Rafey RA, Rudge WE (1994) Phys Rev Lett 73:272
13. Abraham FF, Brodbeck D, Rudge WE, Xu X (1997) J Mech Phys Solids 45:1595
14. Nakano A, Kalia RK, Vasishta P (1995) Phys Rev Lett 75:3138
15. Kalia RK, Nakano A, Omeltchenko A, Tsuruta K, Vashishta P (1997) Phys Rev Lett 78:2144
16. Van Brutzel L, Rountree CL, Kalia RK, Nakano A, Vashishta P (2002) In: Materials research society symposium proceedings April 2002, MRS, 2002, Vol. 703 p. 117
17. Wiederhorn SM, Bolz LH (1970) J Amer Ceram Soc 53:543
18. Hull D (1997) J Mater Sci 31:1829
19. Dally JW (1979) Exptal Mech 19:749
20. Ma CC, Freund LB (1986) J Appl Mech 53:303
21. Hauch JA, Holland D, Marder M, Swinney HL (1999) Phys Rev Lett 82:3823
22. Gross SP, Fineberg J, Marder M, Mccormick WD, Swinney HL (1993) Phys Rev Lett 71:3162
23. Kalthoff JF (1985) Int J Fracture 27:277
24. Ravi-Chandar K, Knauss WG (1984) Int J Fracture 26:141
25. Soules TF, Busbey RF (1981) J Chem Phys 75:969
26. Ochoa R, Simmons JH (1985) J Non-Cryst Solids 75:413
27. Ochoa R, Swiler TP, Simmons JH (1991) J Non-Cryst Solids 128:57
28. Simmons JH, Swiler TP, Ochoa R (1991) J Non-Cryst Solids 134:179
29. Swiler TP, Simmons JH, Wright AC (1995) J Non-Cryst Solids 182:68
30. Guilloteau E, Charrue H, Creuzet F (1996) Europhys Lett 34:549

31. Celarie F, Prades S, Bonamy D, Ferrero L, Bouchaud E, Guillot C, Marliere C (2003) Phys Rev Lett 90:75504

32. Liebau F (1988) In: Devine RAB (ed) The physics and technology of amorphous SiO2. Plenum, New York, pp 15

33. Haile JM (1992) In: Molecular dynamics simulation: elementary methods. Wiley Inter-Science

34. West JK, Hench LL (1991) J Mater Sci 29:3601

35. Lindsay CG, White GS, Freiman SW, Wong-Ng W (1994) J Am Ceram Soc 77:2179

36. Wong-Ng W, White GS, Freiman SW (1992) J Am Ceram Soc 75:3097

37. Del Bene JE, Runge K, Bartlett RJ (2003) Comp Mat Sci 27:102

38. Kieffer J, Angell CA (1988) J Non-Cryst Solids 106:336

39. Muralidharan Krishna, Simmons JH, Deymier PA, Runge K (2005) J Non-Cryst Solids 351:1532

40. Huff NT, Demiralp E, Cagin T, Goddard WA III (1999) J Non-Cryst Solids 253:133

41. van Beest BWH, Kramer GJ, van Santeen RA (1990) Phys Rev Lett 64:1955; Modifications suggested by L. R. Corrales (private communication)

42. Ewald P (1921) Annln Phys 64:253

43. Hoover WG (1985) Phys Rev A 31:1695; S. Nosé (1984) Mol Phys 52:255

44. Tuckerman ME, Martyna GJ (2000) J Phys Chem B 104:159

45. Wright AC (1993) J Non-Cryst Solids 159:264

46. Allen MP, Tilldesley DJ (1999) In: Computer simulation of liquids. Oxford, UK

47. Proctor BA, Whitney I, Johnson JW (1967) Proc Roy Soc (London) 297A:534

48. France PW, Paradine MJ, Reeve MH, Newns GR (1980) J Mat Sci 15:825

49. Duncan WJ, France PW, Craig SP (1986) In: Strength of inorganic glasses. Plenum, New York, p 309

50. Katz JI (1998) J Appl Phys 84:1928

51. Bromley ST, Zwijnenburg MA, Maschmeyer Th (2003) Phys Rev Lett 90:35502

52. Ceresoli D, Bernasconi M, Iarlori S, Parrinello M, Tosatti E (2000) Phys Rev Lett 84:3887

53. Roder A, Kob W, Binder K (2001) J Chem Phys 114:7602

54. Ferrari AM, Garrone E, Spoto G, Ugliengo P, Zecchina A (1995) Surf Sci 323:151

55. Bunker BC, Haaland DM, Michalske TA, Smith WL (1981) Surf Sci 222:95